Fish and Shellfish Immunology 90 (2019) 385–394

Contents lists available at ScienceDirect

Fish and Shellfish Immunology

journal homepage: www.elsevier.com/locate/fsi

Full length article

Integrated transcriptome analysis of immunological responses in the pearl sac of the triangle sail mussel (*Hyriopsis cumingii*) after mantle implantation

Dandan Huang[a,1], Jiexuan Shen[a], Jiale Li[a,b,c,**], Zhiyi Bai[a,b,c,*]

[a] Key Laboratory of Genetic Resources for Freshwater Aquaculture and Fisheries, Shanghai Ocean University, Ministry of Agriculture, Shanghai, 201306, China
[b] Shanghai Engineering Research Center of Aquaculture, Shanghai Ocean University, Shanghai, 201306, China
[c] Shanghai Collaborative Innovation for Aquatic Animal Genetics and Breeding, Shanghai, 201306, China

ARTICLE INFO

Keywords:
Hyriopsis cumingii
Mantle implantation
Pearl sac
Transcriptome
Immunological response

ABSTRACT

For pearl culture of bivalve *Hyriopsis cumingii*, implantation of the sabio may cause nucleus discharge and increased host death rates. We performed a transcriptome analysis of the pearl sac of *H. cumingii* for 30 days after mantle implantation; 293863 unigenes were obtained, and 27176 unigenes were identified using nr, nt, KO, Swiss-Prot, Pfam, GO, and KOG databases. We detected 4878 differentially expressed genes (DEGs) through pairwise comparisons. We speculated that the physical condition of the recipient mussels returned to normal in about one month; the period was divided into six vital phases (0, 2 h–6 h, 12 h–24 h, 48 h to 7 days, 14 days and 30 days) on the basis of the overall similarities in DEGs. We compared the DEGs between time points and identified key immune-related genes. Our findings provide information on the immunological reactions induced by implantation in pearl mussels.

1. Introduction

The triangle sail mussel, *Hyriopsis cumingii*, is the most prevalent and important freshwater pearl-producing mussel in China, accounting for more than 70% yield of freshwater pearls [1]. However, the annual output of pearls is low. In pearl culture, implantation is an indispensable step required for producing pearls. The mantle tissue from donor mussels is cut into small pieces and transplanted into the mantles of recipient mussels, and it proliferates and degenerates into a thin outer epithelial cell layer to form the pearl sac, which secretes and deposits nacre for pearls [2,3]. During healing and regeneration, host mussels are vulnerable to the immune responses to the implantation, resulting in nucleus discharge and higher mortality rate due to the entry of invading pathogenic microorganisms. Pearl culturists have improved the technology for nucleus insertion, but the immunological responses induced by the transplant have not been well alleviated. Therefore, the molecular defense mechanisms induced by implantation in *H. cumingii* need to be investigated to enhance the efficiency of pearl production.

Advances in next-generation sequencing technologies have made it cost-efficient, and the sequence information of many aquatic organisms is available for comprehensive transcriptome analyses. Extensive transcriptome analyses of *Portunus trituberculatus* [4], *Pinctada martensii* [5], *Paralichthys olivaceus* [6], *Cynoglossus semilaevis* [7], and *Crassostrea virginica* [8] have been performed, and many immune-related genes have been identified. The RNA sequencing (RNA-seq) approach is cost-effective and not subjected to the genomic sequences for non-model organism [9,10]. Therefore, RNA-seq method can be applied to obtain more information on existing genetic resources and potential regulatory mechanisms. However, sequence information on *H. cumingii* pearl sacs after implantation has not yet been reported.

Because of the significant economic value of *H. cumingii*, many studies have focused on its immunological responses after mantle implantation. Previous studies on the immune response of *H. cumingii* to grafting analyzed several single genes: HcGal1 [2], HcGal2 [11], AIF-1 [12], HcTRAF6 [13], and interleukin-17 [14]. All these genes have been verified to be involved in pearl sac formation, and they helped us to study the immune defense mechanisms and determine the sampling period of *H. cumingii*. Researchers have clearly shown that mantle pieces from donor mussels that survive immunological rejection can secrete essential biomineralization proteins in host pearl mussels [15].

* Corresponding author. Key Laboratory of Genetic Resources for Freshwater Aquaculture and Fisheries, Shanghai Ocean University, Ministry of Agriculture, Shanghai, 201306, China.
** Corresponding author. Key Laboratory of Genetic Resources for Freshwater Aquaculture and Fisheries, Shanghai Ocean University, Ministry of Agriculture, Shanghai, 201306, China.
E-mail addresses: jlli2009@126.com (J. Li), zybai@shou.edu.cn (Z. Bai).
[1] First author: Dandan Huang.

https://doi.org/10.1016/j.fsi.2019.05.012
Received 29 November 2018; Received in revised form 28 March 2019; Accepted 7 May 2019
Available online 08 May 2019

In this study, we focused on pearl sac formation in *H. cumingii* and performed comprehensive sequencing of transcriptomic changes in the pearl sac for 30 days after mantle implantation. According to the transcriptomic changes, we discovered that it takes 30 days for mantle pieces and donor mussels to return to normal conditions. The periods of 0–2 h, 6 h-12 h, 24 h-48 h, 7 days-14 days, 14 days-30 days generated great changes, so we should particularly pay attention to the aquaculture conditions including water quality, water temperature, and dissolved oxygen during these periods. The specific molecular mechanisms of the identified key genes would be beneficial to the selection of proper immunostimulants during the pearl production. In summary, we utilized the Illumina platform to reveal specific molecular mechanisms against transplant adaptation to pave the way for surrogate pearling.

2. Materials and methods

2.1. Experimental mussels and mantle grafting

In June 2017, healthy mussels were obtained from the experimental base of Xuancheng Farm of Zhexing Pearl Trading Co. Ltd., Anhui Province, China. Mussels of similar size (age, 2 years, shell length, 9–10 cm) were cultured in aeration tanks with recirculating water and fed daily with unicellular algae before the experiment. The implantation was performed by an experienced pearl technician. A strip of mantle tissue (saibo) was dissected from the ventral margin of each donor mussel, cleaned, sterilized, and immediately cut into small rectangular pieces. The rectangular mantle pieces were inserted into the mantles of host mussels by seeding. The transplanted host mussels were placed in the tanks described above for peal sac formation. Total RNA was collected from the pearl sacs at different time points: 2 h, 6 h, 12 h, 24 h, 48 h, 96 h, 7 days, 14 days, and 30 days. The RNA sample from the saibo at 0 h was used as the control. Each RNA sample was obtained from six individual mussels and stored at −80 °C until further analyses.

2.2. RNA isolation, library construction, and illumina sequencing

The total RNA was extracted using TRIzol reagent (Invitrogen, USA), according to the manufacturer's instructions. The RNA samples were checked for degradation and contamination with 1% agarose gel electrophoresis, and RNA concentration and integrity were evaluated using the Qubit RNA assay kit (Life Technologies, USA) and Bioanalyzer 2100 RNA Nano 6000 assay kit (Agilent Technologies, USA), respectively. The pearl sac samples were used to construct the sequencing library with the NEBNext UltraTM RNA Library Prep Kit for Illumina (NEB, USA), according to with manufacturer's instructions, and index codes were assigned to the sequences. In brief, poly(A) mRNA was purified from the total RNA by using oligo-dT-attached magnetic beads. Fragmentation was performed using divalent cations at elevated temperature in NEBNext First Stand Synthesis Reaction Buffer (5×). First-strand cDNA was synthesized using a random hexamer primer and M-MuLV Reverse Transcriptase (RNase H). DNA polymerase I and RNase H were used to synthesize the second-strand cDNA. The quality of the constructed library was assessed with the Agilent 2100 Bioanalyzer. Paired-end cDNA libraries were sequenced using the Illumina HiSeq 2500 system. Image deconvolution and base calling were performed with Illumina CASAVA v1.7.

2.3. Transcriptome assembly and functional annotation

After Illumina sequencing, the raw reads were filtered by excluding the adaptor sequences, reads with ambiguous bases, and low-quality reads. Q20, Q30, and GC content of the clean sequences were calculated. The clean reads were assembled de novo into contigs by using CAP3 [16] with default parameters.

The assembled unigenes (> 100 bp) were determined using BLAST [17] with a significant threshold E-value $< 1 \times 10^{-5}$. The CDS regions were searched and annotated against major databases such as NCBI non-redundant protein (nr), NCBI nucleotide sequences (nt), Swiss-Prot, Kyoto Encyclopedia of Genes and Genomes (KEGG), Eukaryotic Orthologous Groups (KOG), and Pfam. The functional annotations of the unigenes were based on the similarity alignment in the databases. Blast2GO (version 3.1.3) software was used to assign Gene ontology (GO) terms to all the unigenes, and the Web Gene Ontology Annotation Plot (WEGO) software was used for GO functional classification and enrichment analysis.

2.4. Differential expression analysis

The best-aligning result of transcriptome was generated and used as a reference for the downstream analysis after the date processing of de novo assembly. The abundance of unigenes in each sample was estimated using RSEM software with default settings, and the expression levels were normalized and calculated with the RPKM method. The differential expression analysis was based on every pairwise comparison among the samples. The differentially expressed genes (DEGs) were identified using negative binomial distributions of the DEGseq method [18] with the following threshold criteria: $P < 0.01$; $q < 0.001$; and absolute value of log2 ratios (fold change between two groups of pearl sac samples) at > 2. Principle component analysis (PCA) was performed on the basis of the DEG expression levels.

For the enrichment analysis, we mapped all the DEGs to terms in the GO and KEGG databases and described their functions. The RNA-seq library was used as the reference, and the DEGs from each time-point sample were the test sets. We searched for significantly enriched GO and KEGG terms among the DEGs and compared them with the transcriptome background.

2.5. qRT-PCR validation of DEGs

For the qRT-PCR analysis, eight DEGs were selected to verify the reliability of the transcriptome sequencing data. The RNA samples used for the qPCR validation were consistent with those used to construct the transcriptome library. *EF1-α* was used as the endogenous control because its expression level was stable throughout the pearl sac formation [19]. Gene-specific primers for all selected DEGs were prepared using Premier software (version 5.0) and listed in Table 1. We obtained a single product for all the tested genes, and the amplification efficiency was 90–110%. CFX96™ Real-time PCR Detection System (Bio-Rad, USA) was used for the qRT-PCR analysis. The total reaction volume was 20 μL: 10 μL of SYBR Green Master Mix (TaKaRa, Shanghai, China), 0.8 μL each of the forward and reverse primers, 6.8 μL of RNase-free water, and 1.6 μL of cDNA. The cycling parameters were as follows: initial denaturation at 95 °C for 3 min, followed by 40 cycles of amplification at 95 °C for 5 s and 55–60 °C for 30 s. The $2^{-\triangle\triangle CT}$ comparative threshold cycle (Ct) method was used to calculate the relative expression levels of the DEGs. All qPCR reactions were performed in triplicate, and the correlation coefficient (r) values of the expression patterns determined by qRT-PCR and RNA-seq were calculated.

3. Results

3.1. Sequencing and transcriptome assembly

The sequencing data of the pearl sac samples collected at 0 h, 2 h, 6 h, 12 h, 24 h, 48 h, 96 h, 7 days, 14 days, and 30 days were obtained using Illumina paired-end sequencing technology and deposited in the NCBI SRA database under accession number (GSE123069). After data processing, more than 45 million clean reads were obtained for each time point. The data quality assessment showed that more than 99.21% reads from each sample had a q-value ≥20, and more than 94.47% reads had a quality score of Q30. The GC content of the reads from each

Table 1
List of primers used for real-time RT-PCR.

Gene name	Primer name Primer sequence (5′-3′) Application
EF1-α-F	GGAACTTCCCAGGCAGACTGTGC
EF1-α-R	TCAAAACGGGCCGCAGAGAAT
Complement factor B–F	GGCCCATACATGGCGGAAAT
Complement factor B-R	ATCCAGTCGTTCGGGTCACT
Complement component 3-F	AGATGGAAGCCCATGACCGA
Complement component 3-R	ACTGCGTTTGCGTCTTCGAT
Cell division control protein 42-F	GGTGGATCTGAGGGATGATGC
Cell division control protein 42-R	ACAGCACGTAACTCCTTTGCT
MAP kinase-activated protein kinase-2-F	TGGAATGCATGGAGGGTGGA
MAP kinase-activated protein kinase-2-R	AGCTGCTGCCTCTCTCTCTG
Ras-related protein rap-1a-F	TGTTGTTCTAGGAAGTGGAGGTGT
Ras-related protein rap-1a-R	ACACTGCTGGCCATCTACCT
Heat shock protein 90-F	TTGGAAGATCCAGGCACCCA
Heat shock protein 90-R	TCCACTTCCTCCATGCGTGA
cAMP-responsive element binding protein-F	CCCACAGAATTCAGCGCCAT
cAMP-responsive element binding protein-R	ACGCTTCTCCTCTTCCGTGA
B-cell lymphoma 2-F	GTATGCCTTTGCTGCTCGGT
B-cell lymphoma 2-R	CAAACGCATCCCATCCACCA

Table 2
Summary of the transcriptome sequencing data.

Samples	Total raw reads	Total clean reads	Q20%	Q30%	GC content
0 h	55449830	50752124	99.52%	96.06%	44.49%
2 h	53470764	46147544	99.22%	94.47%	45.4%
6 h	55521472	51463490	99.55%	96.32%	46.19%
12 h	51676782	45362130	99.21%	94.69%	44.22%
24 h	55257786	52124130	99.62%	96.9%	46.16%
48 h	56129418	53155822	99.66%	97.08%	43.02%
96 h	55852638	52253440	99.63%	96.77%	43.66%
7D	55902152	53157720	99.70%	97.39%	42.42%
14D	55291678	52003942	99.66%	97.13%	44.18%
30D	54481894	50765740	99.63%	96.83%	44.92%

Table 3
Length distribution statistics of the transcripts and unigenes from the transcriptome.

Transcript length interval	Number of transcripts	Number of unigenes
000-500bp	247667	216789
500-1kbp	49602	43463
1k-2kbp	23247	18626
> 2kbp	18795	14985
Total	339311	293863
Min Length(bp)	34	90
Mean Length(bp)	595	588
Max Length(bp)	30759	27255
N50(bp)	992	840

sample was between 42.42% and 46.19% (Table 2). The obtained data indicated the high quality of the sequencing results and were conducive to the subsequent transcriptome analysis. The length distribution statistics of the transcripts and unigenes from the transcriptome were presented in Table 3. The assembled sequences had a maximum length of 30759 bp and N50 length of 992 bp; 293863 unigenes were obtained, and their mean length was 588 bp and N50 was 840 bp.

3.2. Functional annotation of the assembly

The unigenes assembled from the reads were combined and archived using the BLAST algorithm against the recorded sequences

Table 4
Summary of the annotation statistics of the assembled unigenes.

Database	Number of unigenes	Percentage (%)
NR	23202	7.89
NT	6194	2.11
KO	6466	2.20
SwissProt	19667	6.69
PFAM	13430	4.57
GO	11019	3.75
KOG	13595	4.63
In all databases	1391	0.47
In at least one database	27176	9.25
Total unigenes	293863	100

available in nr, nt, KO, Swiss-Prot, Pfam, GO, and KOG databases (Table 4); 23202, 6194, 6466, 19667, 13430, 11019, and 13595 unigenes were annotated, respectively. A total of 27176 unigenes with a significant hit were identified, and 1391 unigenes could be annotated from all the databases.

The GO term enrichment analysis was performed to obtain information on the functions of the annotated unigenes (Fig. 1) The annotated unigenes were assigned to three major categories: biological process (42.4%), cellular component (22.57%), and molecular function (35.03%); “cellular process,” “membrane,” and “binding” were the most dominant groups, respectively.

To further understand the biological functions of the unigenes in the transcriptome, we mapped all the sequences to pathways in the KEGG database(Fig. 2); 6466 unigenes were assigned to 353 signaling pathways. The KEGG analysis showed that fifteen pathways (Toll-like receptor signaling pathway, NOD-like receptor signaling pathway, Complement and coagulation cascades, etc.) were found to be involved in immune function (Table 5). Amongst these pathways, Toll-like receptor (TLR1、TLR2、TLR4、TLR6), RIG-I-like receptor (retinoic acid inducible gene-1, RIG-1、melanoma differentiation associated gene-5, MDA-5), NOD-like receptor(Neuronal apoptosis inhibitory protein, NAIP), DNA sensor (DNA-dependent activator of IFN-regulatory factor, DAI、RNA polymerase III, RNA Pol III). Innate immunity is the first line of defense against pathogenic invasion in invertebrates [20].

The pathogen-associated molecular patterns (PAMPs), which are expressed on the bacterial surface with highly conserved molecular structures, are recognized by a limited number of germline-encoded pattern-recognition receptors (PRRs) to trigger the innate immune response [21–23]. The identified PRRs function significantly in allograft to suppress the replication of various pathogens in host and decrease the damage caused by the immunological stress.

3.3. Analysis of DEGs

Arrays of genes were identified as DEGs by performing pairwise comparisons of all the samples with a strict distribution algorithm. A total of 4878 genes were determined as significant DEGs, and they showed differential expression profiles in at least one pair of comparison.

The PCA analysis was performed, and the sum of PC1 and PC2 was attributable to 58.5% of the variance (Fig. 3); hence, dimensionality reduction was achieved. Heat map analysis was used to define clusters of DEGs on the basis of their differential expression profiles (Fig. 4). The hierarchical clustering results revealed that DEGs obtained from the samples at 2 h and 6 h; 12 h and 24 h; 48 h, and 96 h and 7 days had similar clustering and expression characteristics. Both PCA and clustering analysis revealed that the expression patterns at time points 0 h and 30 days were similar. Therefore, we speculated that the physical condition of the recipient mussels and donor mantle pieces returned to normal after implantation for about one month, which was divided into six vital phases (0, 2–6 h, 12–24 h, 48 h to 7 days, 14 days, and 30 days)

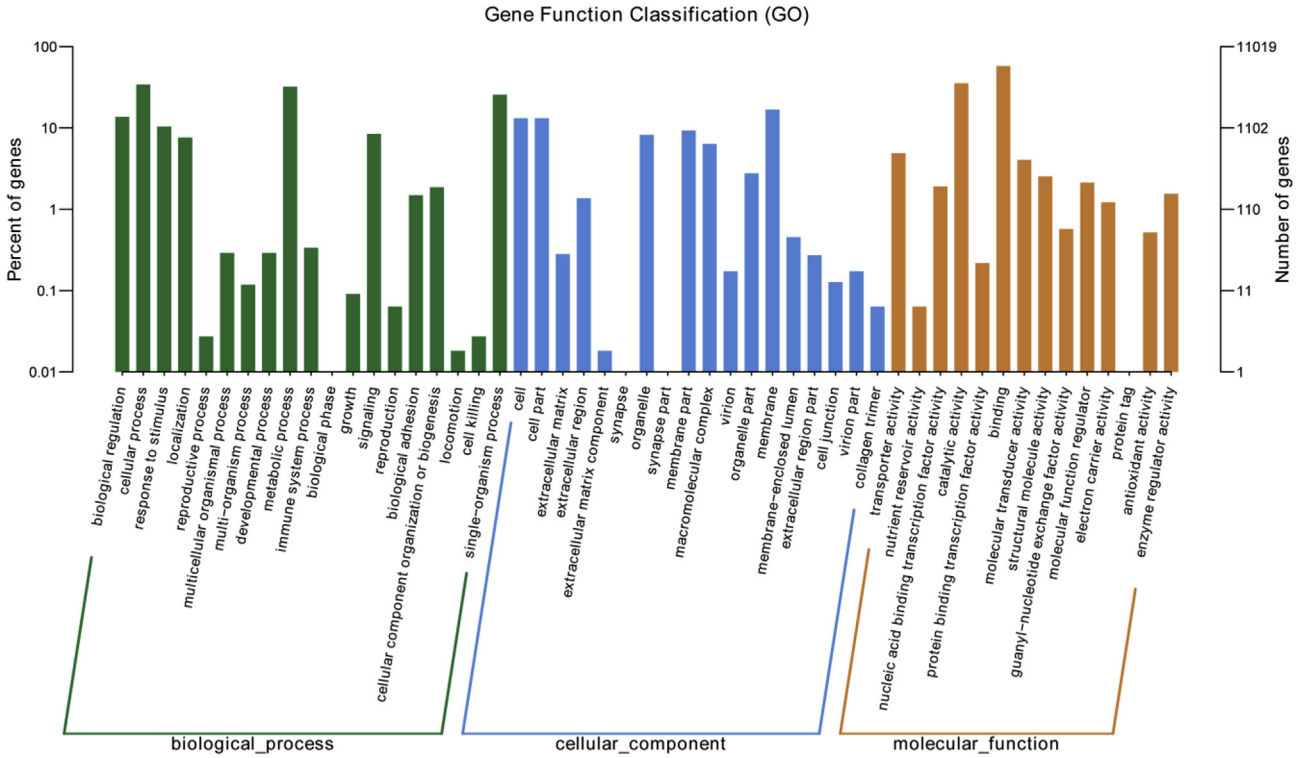

Fig. 1. Gene ontology (GO) classification of the annotated unigenes.

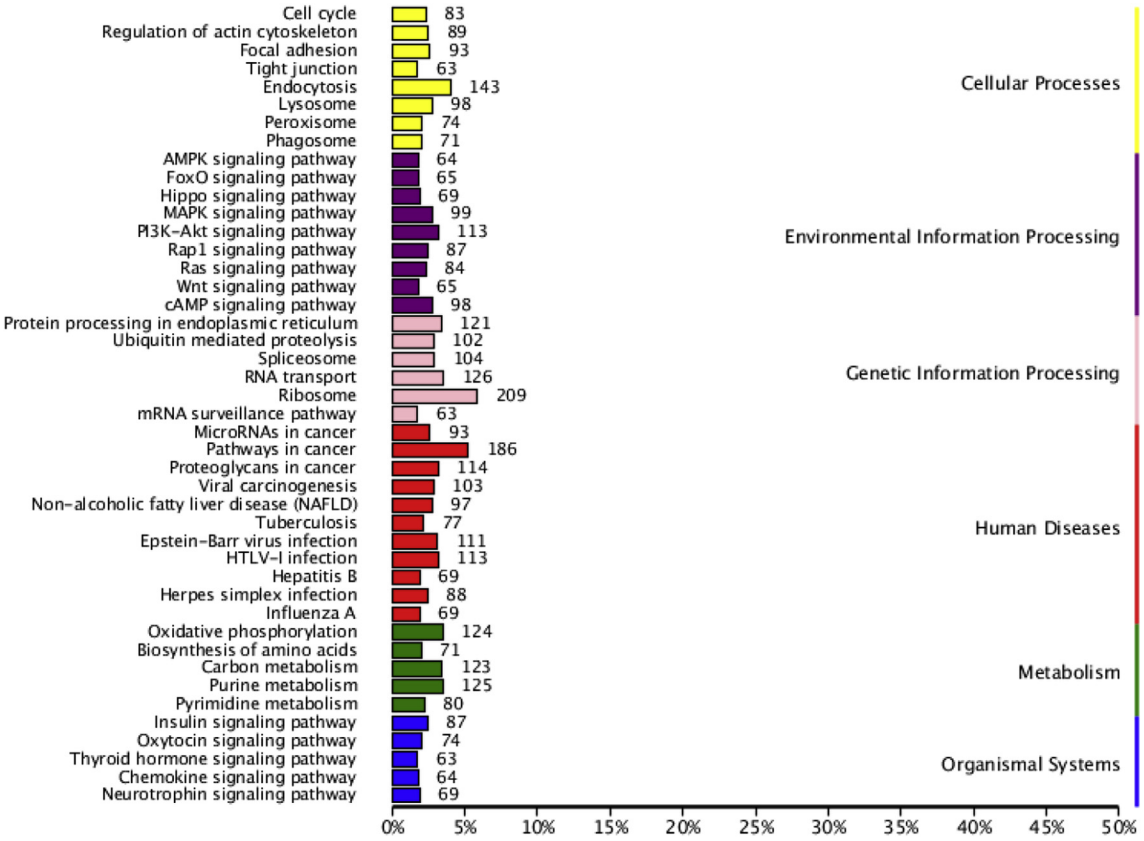

Fig. 2. KEGG pathway classification of the assembled unigenes.

on the basis of the overall similarities in the DEGs among the samples. We compared the DEGs between 0/2 h, 6 h/12 h, 24 h/48 h, 7 days/14 days, and 14 days/30 days to gain an insight of the dynamic physiological changes that occur in mussels during pearl sac formation.

Table 5
Fifteen immune-related KEGG signaling pathways.

KEGG pathways	Number of unigenes	Pathway ID
Antigen processing and presentation	24	ko04612
B cell receptor signaling pathway	43	ko04662
Chemokine signaling pathway	64	ko04062
Complement and coagulation cascades	12	ko04610
Cytosolic DNA-sensing pathway	32	ko04623
Fc epsilon RI signaling pathway	26	ko04664
Fc gamma R-mediated phagocytosis	44	ko04666
Hematopoietic cell lineage	4	ko04640
Leukocyte transendothelial migration	38	ko04670
NOD-like receptor signaling pathway	30	ko04621
Natural killer cell mediated cytotoxicity	31	ko04650
Platelet activation	56	ko04611
RIG-I-like receptor signaling pathway	30	ko04622
T cell receptor signaling pathway	47	ko04660
Toll-like receptor signaling pathway	45	ko04620

3.4. Identification and enrichment analysis of DEGs

Dynamic changes in the expression levels of the DEGs obtained from the five pairwise comparisons were evaluated and summarized in Fig. 5. In the 0 h/2 h pairwise comparison, 632 genes were found to be differentially expressed, namely, 395 upregulated genes and 237 downregulated genes. The total number of DEGs increased in the following comparisons and was 1846 in the 14 days/30 days group. Simultaneously, the significant downregulation of genes in comparison of 14 days/30 days were consistent with the heatmap analysis, supporting that the expression levels of unigenes were similar at 0 h and 30 days, and the host physical condition returned to normal for about one month. GO and KEGG enrichment analyses of the DEGs were performed to identify the over-represented terms and key genes in the immune response.

In the 6 h/12 h pairwise comparison, functional GO terms such as chitin metabolic process (GO: 0006030), response to biotic stimulus (GO: 0009607), and small GTPase-mediated signal transduction (GO: 0007264) were found to be significantly enriched. In the 0 h/2 h pairwise comparison, chitin metabolic process was the most significantly enriched. Many DEGs in the 24 h/48 h and 7 days/14 days groups were associated with translation (GO: 0006412), oxidation-reduction process

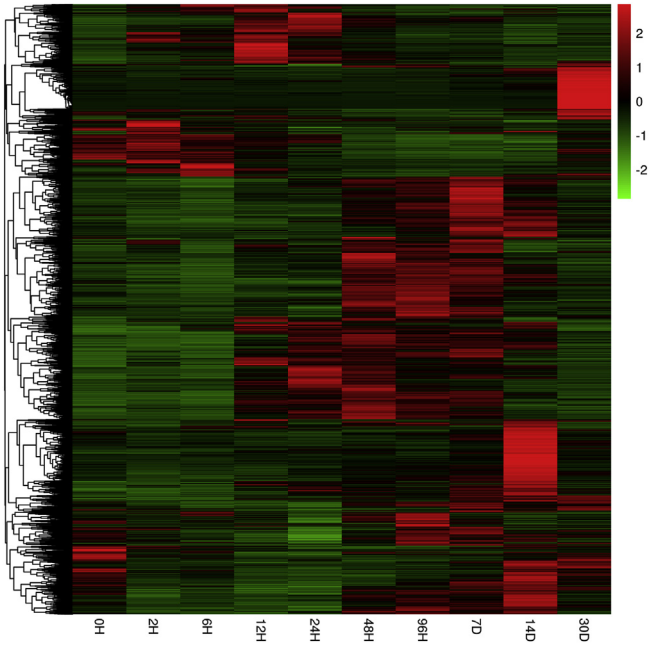

Fig. 4. Hierarchical clustering analysis of the differentially expressed genes (DEGs) at the 10 time points. A log10 scale was used to normalize the gene signal intensities in the heat map analysis.

(GO: 0055114), response to oxidative stress (GO: 0006979), superoxide metabolic process (GO: 0034622), etc., and some of them were involved in immunological processes. In the 14 days/30 days group, a large number of genes were associated with the immune system process (GO: 0006955), defense response (GO: 0006952), and homeostatic process (GO: 0042592).

The KEGG pathway analysis indicated 40 significantly enriched pathways in 0 h/2 h group, and most of the pathways were involved in immune functions such as Leukocyte transendothelial migration, T cell receptor signaling pathway, Complement and coagulation cascades, Wnt signaling pathway, B cell receptor signaling pathway, Phagosome, Fc gamma R-mediated phagocytosis, TNF signaling pathway, and

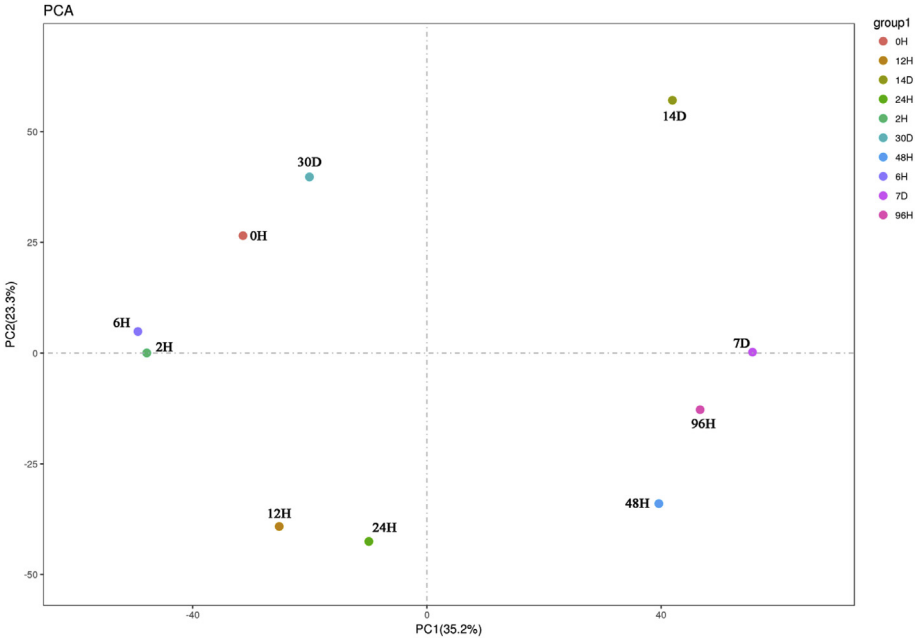

Fig. 3. Principle component analysis (PCA) of the differentially expressed genes (DEGs) in the 10 samples.

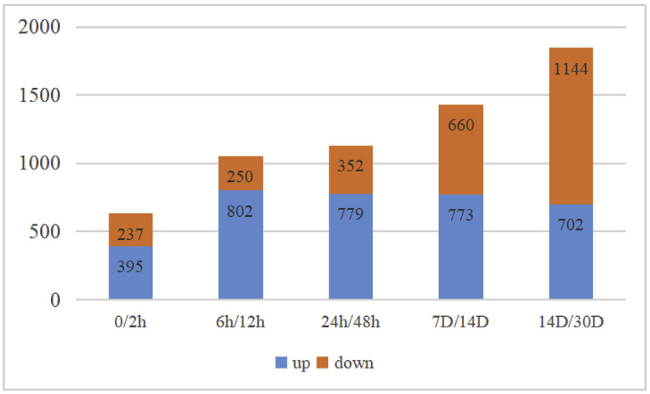

Fig. 5. Pairwise comparisons of the expression levels of differentially expressed genes (DEGs) at 0, 2 h–6 h, 12 h–24 h, 48 h to 7 days, 14 days, and 30 days. The orange and blue in each column represent the number of downregulated and upregulated transcripts. (For interpretation of the references to color in this figure legend, the reader is referred to the Web version of this article.)

Platelet activation. Notably, Complement and coagulation cascades were found to be enriched in four pairwise comparisons (0 h/2 h, 24 h/48 h, 7 days/14 days, and 14 days/30 days). Oxidative phosphorylation was the most represented pathway in the 24 h/48 h group. The mitogen-activated protein kinase (MAPK) signaling pathway was found to be differentially expressed in all pairwise comparisons and significantly enriched in 6 h/12 h and 7 days/14 days.

3.5. qRT-PCR validation of DEGs

To confirm the accuracy of the gene expression profiles in our transcriptome, eight DEGs were selected from the assembled sequences for the qRT-PCR analysis. The fold changes at each time point after the implantation by qRT-PCR analysis were compared against the RNA-seq expression profiles (Fig. 6). The significant correlation coefficient (r) values of the expression patterns determined with qRT-PCR and RNA-seq ranged from 0.86 to 0.97, demonstrating that the expression patterns of the selected DEGs determined by the two methods were identical. The results provided convincing evidence that the transcriptomic profiles were accurate and reliable.

4. Discussion

H. cumingii is commonly used to produce non-nucleus pearls via mantle implantation, which may lead to major immunological responses to allografts and pathogen infections. To the best of our knowledge, this is the first survey of the transcriptomic responses in the pearl sac of *H. cumingii* to mantle implantation over a period of 30 days to understand the functions and identify the key molecules related to the immune reaction. In addition, the mussels were on normal rations and there was no death during the whole experiment.

The transcriptome sequencing yielded a total of 293863 unigenes with a mean length of 588 bp and N50 length of 840 bp, and 27176 assembled unigenes were matched to homogeneous sequences in at least one database. GO and KEGG functional analyses revealed abundant immune-related genes, illustrating a complicated immune system response to implantation in the pearl sacs of the recipient mussels. It was predicted that pearl sac was formed at about 12 days [24] and then the stage was for nacre secretion. The PCA and hierarchical clustering analysis were conducted based on dynamic expression changes at various time points of 4878 DEGs obtained using comparative transcriptomic analysis. On the basis of the results, we speculated that the recipient mussels underwent several major stages of adjustment, and the period after implantation was divided into six vital phases (0, 2–6 h, 12–24 h, 48 h to 7 days, 14 days, and 30 days). We compared the DEG levels at 0/2 h, 6 h/12 h, 24 h/48 h, 7 days/14 days, and 14 days/30 days and performed GO and KEGG pathway enrichment analyses of the five groups to investigate the molecular mechanisms and hub gene-induced immune tolerance during pear sac formation.

4.1. Complement and coagulation cascades

Our study showed that the complement and coagulation cascades were significantly enriched, elucidating that the DEGs associated with the cascades have vital functions at the onset of pearl formation. The complement and coagulation cascades act locally, namely, activated complement was implicated with the site of infection and coagulation was involved in the part of bleeding [25]. Damage to the organism or microbial infections activate these cascades via serine proteases, which are the common ancestors of the complement and coagulation systems [25]. In this study, the expression level of the serine protease inhibitor (SPI) was significantly upregulated by 4.92–52.79-fold from 2 h to 14 days. The data indicated that SPI in pearl sacs can accurately mediate the protease cascade reaction in *vivo* to prevent the activation of excessive serine proteases and suppress protease activities on the surface of the host and resist invading pathogens [26–28].

The complement system is a major component of innate immunity and a bridge between innate and adaptive immune responses against infection in vertebrates [29–31]. The complement system has crucial functions via a broad spectrum of immunological regulatory mechanisms, such as inflammation, phagocytosis, apoptotic, cytolysis, and humoral immune responses [32]. Activation of the complement system requires three convergent pathways: classical, lectin, and alternative [33]. In our study, complement component 3 (C3) and complement factor B (CFB) were assumed as the key genes, and CFB and C3 exhibited similar expression patterns throughout the experimental period. Their expression levels initially decreased slightly in 24 h, dramatically declined up to 14 days, and eventually returned to normal. The metabolic level of donor mantle pieces and recipient mussels was in a poor condition accompanied by the body damage and bacteria invasion. Hence, the recipient mussels decreased autoimmune activities for self-defense with the down-regulation of key immune-related genes in the preliminary stage.

The coagulation system is a part of the homeostatic process. In this study, transglutaminase, prothrombin, and fibrinogen-related protein orthologues were found amongst the coagulation factors, and they exhibited similar expression patterns that peaked around 14 days. The results of western bolt showed that the expression of coagulation factor in crab(*Eriocheir sinensis*)was significantly induced in heart, hepatopancreas and blood after the infection of bacterium and artificial fracture. It was concluded that coagulation factor in crab could boost clotting, and catalytic fibrinogen into fibrin to prevent the spread of pathogens or toxic substances [34]. It has also been demonstrated that prothrombin cleaves fibrinogen to form fibrin clots, decreasing the spread of bacteria in vertebrates [35]. Therefore, we speculated that the upregulation of prothrombin was likely to contribute to protein synthesis and facilitate the ability of cleaving fibrinogen and resisting the invasion of pathogenic bacteria post mantle implantation.

4.2. MAPK signaling pathway

The genes in the MAPK signaling pathway were found to differently express in all comparisons and significantly enriched at 6 h/12 h and 7 days/14 days. MAPK cascades are highly conserved in yeast and humans, and they are responsible for the intracellular signaling associated with various cellular functions, such as transformation, apoptosis, and cell differentiation and proliferation [36–38]. The characteristic core unit is a series of three sequentially activating kinases: MAPK kinase kinase (MAPKKK), MAPK kinase (MAPKK), and MAPK [39]. MAP kinase-activated protein kinase-2 (MAPKAPK-2), heat-shock protein (HSP)-70, filamin A, MAP kinase-interacting serine/threonine-protein

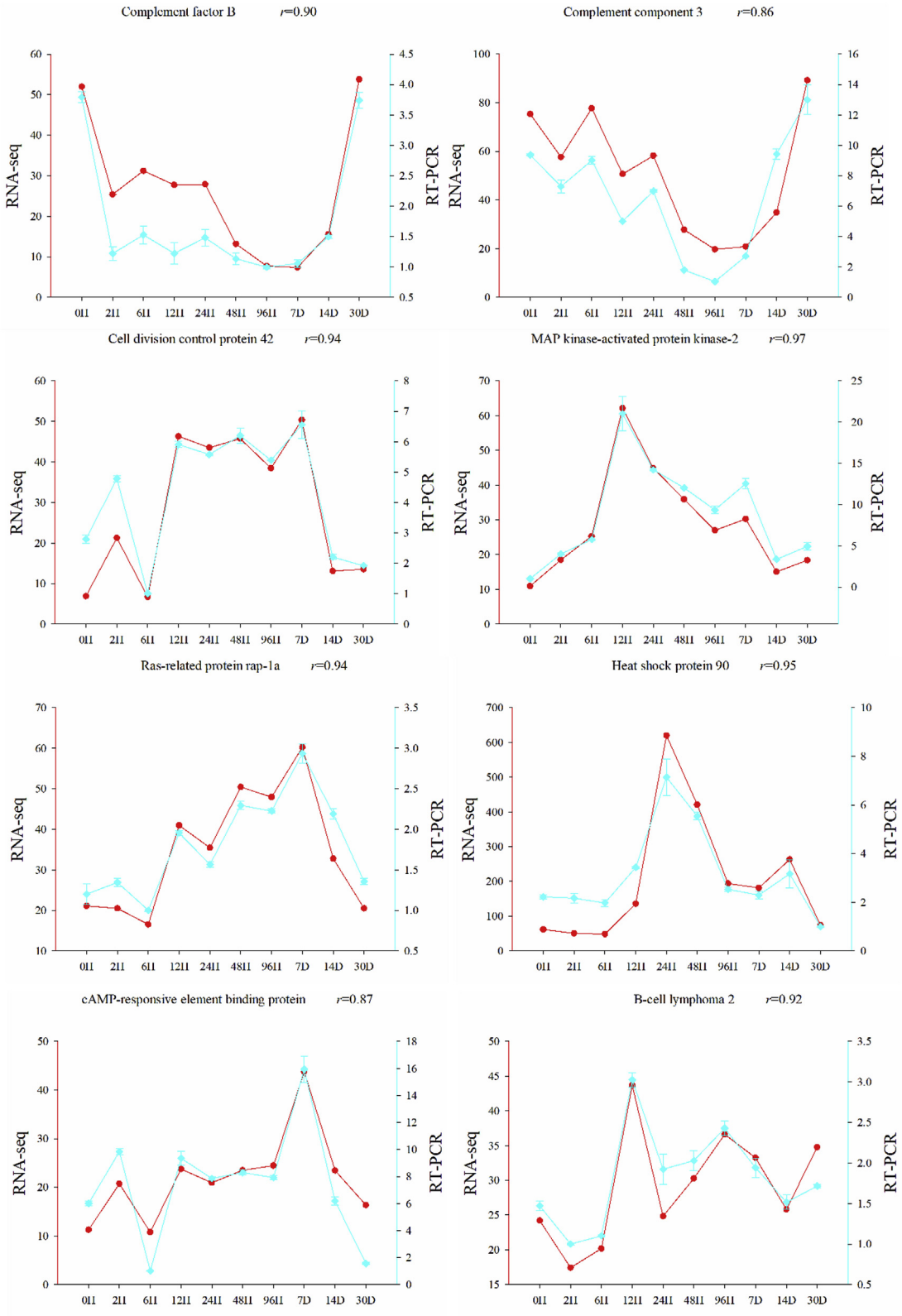

Fig. 6. Comparisons of the expression profiles determined using qRT-PCR and transcriptome sequencing. The red lines represent RNA-seq results, and the blue represent qRT-PCR results. (For interpretation of the references to color in this figure legend, the reader is referred to the Web version of this article.)

kinase 1 (MKNK1), cell division control protein 42 homolog isoform 1, and ras-related protein rap-1a were significantly enriched in 6 h and 12 h. Although the expression patterns of the genes differed, the expression levels collectively showed a remarkable increase at 12 h when compared with that at 6 h. The rapid response of the MAPK cascade was sensitive to the external stimulus caused by the mantle grafting. A previous study on the pearl oyster *Pinctada maxima* reported that the MAPK signaling pathway was associated with the immune rejection of the xenograft by the host [40]. MAPKAPK-2 plays a crucial role in the inflammation process, which is required to accelerate wound healing

after an injury [41]. In our study, the upregulation of MAPKAPK-2 demonstrated its role in wound healing mediated by the p38/MAPKAPK-2 signaling pathway after the implantation.

Small GTP-binding proteins (G proteins) are monomeric guanine nucleotide-binding proteins [42]. GTPases of the RAS superfamily are molecular switches that are capable of regulating multiple functions, such as signal transduction, cell division, proliferation, and cytoskeleton control and motility, and they can be structurally divided into several smaller subfamilies: Rab, Rho, Ras, Ran, and Arf/Sar [43]. In this study, Rap1, Rho, and cdc42 all showed high expression continuously at the experimental time points. The Ras family protein Rap1 acts as the key regulator in activating integrin-mediated adhesion and cell proliferation mediated by extracellular stimulus [44,45]. Rap1 has been reported to be involved in immune reactions in invertebrates [46,47]. Rho1 and cdc42 are Rho family members, and they coordinate the wound repair mechanism by accumulating around the wound and rapidly separating it into dynamic zones [48]. However, their specific repair mechanism during pearl sac formation is unknown and needs to be studied in the future.

4.3. PI3K-Akt signaling pathway

The PI3K-Akt signaling cascade affects broad aspects of biological processes such as cell survival, growth, differentiation, migration, and, especially, apoptosis [49]. The cascade plays a key role in resisting external stimulation by the environment and pathogen infection from vertebrates to invertebrates [49,50]. In *Haliotis diversicolor*, the PI3K-Akt pathway was detected to have an efficient molecular mechanism in response to pathogen infections under hypoxia, thermal, and thermal plus hypoxia conditions [51]. HSP90 acts as a molecular chaperone that is indispensable for maintaining the stability and functions of protein conformations, and it is a protective molecule closely related to stress tolerance [51]. The mRNA of HSP90 in *Portunus trituberculatus* [52] and *Mytilus coruscus* [53] was upregulated under different environmental stress. In this study, the expression profile of HSP90 at 12 h, 24 h, 48 h, 96 h, 7 days, and 14 days was notably upregulated. Therefore, we infer that, in the PI3K-Akt signaling cascade, HSP90 plays a major role in physiological and stressful conditions induced by the implantation. Moreover, the high expression of B-cell lymphoma 2 showed that it could inhibit the apoptosis caused by diverse induction factors during pearl sac formation [54].

Wound healing in the host mussels and the formation of pearl sacs from mantle pieces are complex events and involve processes such as cell differentiation, migration, and proliferation [55]. Microfibril-associated glycoprotein 4, fibril-forming collagen alpha, cartilage oligomeric matrix protein, cartilage matrix protein, and collagen alpha-2(IV) all belong to the extracellular matrix [56] and exhibit dynamic expression changes that require integrins to allow cell migration and differentiation [57]. Our data revealed that the transcriptional level of integrin β subunit began to increase and peaked at 7 days. New insights into the role of integrins in the invertebrate immune system have demonstrated their involvement in phagocytosis, melanization, and encapsulation [58,59]. These cell–matrix interactions lead to the activation of downstream reactions, and the transcription factor cAMP-responsive element binding protein, which affects the expression of survival genes, is mediated by Akt [60]. Collectively, the PI3K-Akt cascade plays an essential role in the regulation of cell apoptosis, wound healing, and immune responses after mantle implantation. These molecules interact with each other and can be induced by the physical changes in host mussels after grafting.

4.4. Chitin metabolic process

The GO enrichment analysis showed that the chitin metabolic process (GO: 0006030) was significantly enriched in all the tested comparisons, except 7 days/14 days. Chitin, a linear and unbranched aminopolysaccharide, is composed of *N*-acetylglucosamine monomers [61]. The nacreous layer is composed of 95% calcium carbonate and 5% matrix proteins, including chitin, and they contribute to the dominant regulatory mechanisms underlying biomineralization [62]. Suzuki and Nagasawa (2009) proposed a model for the formation of the nacreous layer, and they elucidated that chitin can probably form a bigger aggregate with other proteins in this process [63]. Hence, chitins are indispensable for pearl formation by mollusks. Currently, many genes that encode chitinases have been identified and characterized in mollusks because of their importance in shell and nacre formation [64–66]. *Cg*-Clp1, *Cg*-Clp2, and *Cg*-Chit from *Crassostrea gigas* were found to play crucial regulatory roles in embryonic development, tissue remodeling, and adult oyster growth [64].

Our data showed that 18 DEGs were enriched in the chitin metabolic process. According to the detected dynamic expression levels of these unigenes throughout the experimental period, two major groups were formed: one group was upregulated before the time point of 14 days, and the other group was very abundant in 30 days. In pearl oysters, mineral deposition during pearl formation is divided into two stages: irregular and regular deposition [67]. The expression of major genes enriched during the chitin metabolic process mainly increased in the irregular deposition stage, regulating the nucleation of calcium carbonate; the high expression of endochitinase was detected in the preliminary stage of the pearl sac formation. The insoluble organic framework is formed by chitins and provides structural support for crystal nucleation and growth [68]. We speculated that endochitinase modified and degraded excess chitins to maintain the orderliness of the framework. Five unigenes were all observed to have conserved domains: chitin-binding domain type 2 and chitin-binding domain peritrophic-A domain; barely expressed before 14 days; and dramatically peaked at 30 days. Previous studies from our laboratory have proven that the shiny luster appears at around 21 days after mantle implantation [62,69]. The high expression levels of these genes at 30 days suggest their participation in the regular deposition stage and nacreous layer formation. These genes related to biomineralization supplement our knowledge on the morphological and physiological changes of the pearl sacs after mantle grafting.

5. Conclusions

To the best of our knowledge, this is the first survey of transcriptional changes in the pearl sacs of *H. cumingii* across 30 days in response to mantle implantation by using RNA-seq technology. PCA and hierarchical clustering analysis showed that the physical condition of the recipient mussels and donor mantle pieces returned to normal in about one month on the basis of the expression profiles of DEGs at various time points. The comparative transcriptomic analysis helped us to divide the experimental period into six vital phases (0, 2–6 h, 12–24 h, 48 h to 7 days, 14 days, and 30 days) and identify key genes in the complement and coagulation cascades, MAPK signaling pathway, PI3K-Akt signaling pathway, and chitin metabolic process. In the present study, the transcriptome data help us find that there were great changes occurred in the comparisons of 0/2 h, 6 h/12 h, 24 h/48 h, 7 days/14 days, and 14 days/30 days. Hence, we should take notice of the aquaculture conditions including water quality, water temperature, and dissolved oxygen at these key time points, particularly the entry of invading pathogenic microorganisms. Meanwhile, some genes related to immune tolerance were identified by the investigations of enriched GO terms and KEGG pathways of the DEGs. The specific molecular mechanisms post mantle implantation also laid the theoretical foundation for the selection of proper immunostimulants. Overall, these appropriate treatments would reduce the risk of infection and nucleus discharge during pearl sac formation.

Acknowledgements

Our work was supported by the Chinese Ministry of Science and Technology through the National Key Research and Development Program of China (2018YFD0901406), the earmarked fund for Modern Agro-industry Technology Research System (CARS-49), the National Natural Science Foundation of China (31672654), and the Project of Shanghai Engineering and Technology Center for Promoting Ability (16DZ2281200). Additionally, we were grateful to Dr Maoxiao Peng for his help.

References

[1] J. Li, Y. Li, Aquaculture in China–freshwater Pearl Culture, World Aquacult, 2009.
[2] Z. Bai, L. Zhao, X. Chen, Q. Li, J. Li, A galectin from *Hyriopsis cumingii* involved in the innate immune response against to pathogenic microorganism and its expression profiling during pearl sac formation, Fish Shellfish Immunol. 56 (2016) 127–135.
[3] D. Hua, R.J. Neves, Captive survival and pearl culture potential of the pink *Heelsplitter potamilus* alatus, N. Am. J. Aquacult. 69 (2007) 147–158.
[4] J. Lv, P. Liu, Y. Wang, B. Gao, P. Chen, J. Li, Transcriptome analysis of Portunus trituberculatus in response to salinity stress provides insights into the molecular basis of osmoregulation, PLoS One 8 (2013) e82155.
[5] W. Wang, Y. Wu, Q. Lei, H. Liang, Y. Deng, Deep transcriptome profiling sheds light on key players in nucleus implantation induced immune response in the pearl oyster *Pinctada martensii*, Fish Shellfish Immunol. 69 (2017) 67–77.
[6] Z. Li, X. Liu, J. Cheng, Y. He, X. Wang, Z. Wang, et al., Transcriptome profiling provides gene resources for understanding gill immune responses in Japanese flounder (Paralichthys olivaceus) challenged with *Edwardsiella tarda*, Fish Shellfish Immunol. 72 (2018) 593–603.
[7] X. Zhang, S. Wang, S. Chen, Y. Chen, Y. Liu, C. Shao, et al., Transcriptome analysis revealed changes of multiple genes involved in immunity in *Cynoglossus semilaevis* during *Vibrio anguillarum* infection, Fish Shellfish Immunol. 43 (2015) 209–218.
[8] L. Zhang, L. Li, Y. Zhu, G. Zhang, X. Guo, Transcriptome analysis reveals a rich gene set related to innate immunity in the Eastern oyster (*Crassostrea virginica*), Mar. Biotechnol. 16 (2014) 17–33.
[9] X.W. Wang, J.B. Luan, J.M. Li, Y.L. Su, J. Xia, S.S. Liu, Transcriptome analysis and comparison reveal divergence between two invasive whitefly cryptic species, BMC Genomics 12 (2011) 458.
[10] C.C. Sánchez, G.M. Weber, G. Gao, B.M. Cleveland, J. Yao, C.E.R. Iii, Generation of a reference transcriptome for evaluating rainbow trout responses to various stressors, BMC Genomics 12 (2011) 626.
[11] Z. Bai, L. Zhao, X. Chen, Q. Li, J. Li, A galectin contributes to the innate immune recognition and elimination of pathogens in the freshwater mussel *Hyriopsis cumingii*, Dev. Comp. Immunol. 73 (2017) 36–45.
[12] Q. Li, Z. Bai, L. Zhao, J. Li, Characterization of allograft inflammatory factor-1 in *Hyriopsis cumingii* and its expression in response to immune challenge and pearl sac formation, Fish Shellfish Immunol. 59 (2016) 241–249.
[13] D. Huang, Z. Bai, J. Shen, L. Zhao, J. Li, Identification of tumor necrosis factor receptor-associated factor 6 in the pearl mussel *Hyriopsis cumingii* and its involvement in innate immunity and pearl sac formation, Fish Shellfish Immunol. 80 (2018) 335–347.
[14] R. Zhang, M. Wang, N. Xia, S. Yu, Y. Chen, N. Wang, Cloning and analysis of gene expression of interleukin-17 homolog in triangle-shell pearl mussel, *Hyriopsis cumingii*, during pearl sac formation, Fish Shellfish Immunol. 52 (2016) 151–156.
[15] E.L. McGinty, K.R. Zenger, D.B. Jones, D.R. Jerry, Transcriptome analysis of biomineralisation-related genes within the pearl sac: host and donor oyster contribution, Mar Genom 5 (2012) 27–33.
[16] X. Huang, A. Madan, CAP3: a DNA sequence assembly program, Genome Res. 9 (1999) 868.
[17] S.F. Altschul, W. Gish, W. Miller, E.W. Myers, D.J. Lipman, Basic local alignment search tool, J. Mol. Biol. 215 (1990) 403–410.
[18] S. Anders, W. Huber, Differential expression analysis for sequence count data, Genome Biol. 11 (2010) R106.
[19] Z. Bai, J. Lin, K. Ma, G. Wang, D. Niu, J. Li, Identification of housekeeping genes suitable for gene expression analysis in the pearl mussel, *Hyriopsis cumingii*, during biomineralization, Mol. Genet. Genom. 289 (2014) 717–725.
[20] D.A. Kimbrell, B. Beutler, The evolution and genetics of innate immunity, Nat. Rev. Genet. 2 (2001) 256–267.
[21] E. Meylan, J. Tschopp, M. Karin, Intracellular pattern recognition receptors in the host response, Nature 442 (2006) 39.
[22] T.H. Mogensen, Pathogen recognition and inflammatory signaling in innate immune defenses, Clin. Microbiol. Rev. 22 (2009) 240–273.
[23] S. Akira, S. Uematsu, O. Takeuchi, Pathogen recognition and innate immunity, Cell 124 (2006) 783–801.
[24] C. Jin, J.-Y. Zhao, X.-J. Liu, J.-L. Li, Expressions of shell matrix protein genes in the pearl sac and its correlation with pearl weight in the first 6 Months of pearl formation in *Hyriopsis cumingii*, Mar. Biotechnol. (2019) 1–10.
[25] M.M. Markiewski, B. Nilsson, K.N. Ekdahl, T.E. Mollnes, J.D. Lambris, Complement and coagulation: strangers or partners in crime? Trends Immunol. 28 (2007) 184–192.
[26] G. Simonet, I. Claeys, J.V. Broeck, Structural and functional properties of a novel serine protease inhibiting peptide family in arthropods Comp, Biochem Phys B 132 (2002) 247–255.
[27] M.M. Krem, C.E. Di, Evolution of enzyme cascades from embryonic development to blood coagulation, Trends Biochem. Sci. 27 (2002) 67–74.
[28] D. Scott, Complement in Health and disease. Immunology and medicine, J. Clin. Pathol. 40 (1987) 1488–e.
[29] K. Yang, Complement: a key system for immune surveillance and homeostasis, Nat. Immunol. 11 (2010) 785.
[30] H. Molina, Complement and immunity, Rheum. Dis. Clin. N. Am. 30 (2004) 1–18.
[31] J.E. Volanakis, M.M. Frank, The Human Complement System in Health and Disease, Crc Press, 1998.
[32] B.Z. Schmidt, H.R. Colten, Complement: a critical test of its biological importance, Immunol. Rev. 178 (2010) 166–176.
[33] M. Wills-Karp, Complement activation pathways: a bridge between innate and adaptive immune responses in asthma, Proc. Am. Thorac. Soc. 4 (2007) 247.
[34] cDNA Cloning and Expression Patternsof Coagulation Factorin *Eriocheir Sinensis*, Soochow University, 2016.
[35] H. Sun, The interaction between pathogens and the host coagulation system, Physiology 21 (2006) 281.
[36] T. Nakahara, Y. Moroi, H. Uchi, M. Furue, Differential role of MAPK signaling in human dendritic cell maturation and Th1/Th2 engagement, J. Dermatol. Sci. 42 (2006) 1–11.
[37] E.K. Kim, E.J. Choi, Pathological roles of MAPK signaling pathways in human diseases, Bba-Mol Basis Dis. 1802 (2010) 396–405.
[38] A.S. Dhillon, S. Hagan, O. Rath, W. Kolch, MAP kinase signalling pathways in cancer, Oncogene 26 (2007) 3279–3290.
[39] T.P. Garrington, G.L. Johnson, Organization and regulation of mitogen-activated protein kinase signaling pathways, Curr. Opin. Cell Biol. 11 (1999) 211–218.
[40] J. Wei, S. Fan, B. Liu, B. Zhang, J. Su, D. Yu, Transcriptome analysis of the immune reaction of the pearl oyster *Pinctada fucata* to xenograft from *Pinctada maxima*, Fish Shellfish Immunol. 67 (2017) 331–345.
[41] T. Thuraisingam, Y.Z. Xu, K. Eadie, M. Heravi, M.C. Guiot, R. Greemberg, et al., MAPKAPK-2 signaling is critical for cutaneous wound healing, J. Investig. Dermatol. 130 (2010) 278–286.
[42] H.H. Jensen, F.H. Login, J.Y. Park, T.H. Kwon, L.N. Nejsum, Immunohistochemical evaluation of activated Ras and Rac1 as potential downstream effectors of aquaporin-5 in breast cancer in vivo, Biochem Biophys Res Co 493 (2017) 1210–1216.
[43] K. Wennerberg, K.L. Rossman, C.J. Der, The Ras superfamily at a glance, J. Cell Sci. 118 (2005) 843–846.
[44] E. S, H.A. Rho, GTPases in cell biology, Nature 420 (2002) 629–635.
[45] D.S. Johnson, Y.H. Chen, Ras family of small GTPases in immunity and inflammation, Curr. Opin. Pharmacol. 12 (2012) 458–463.
[46] X. Huang, T. Ye, M. Jin, W. Wang, K. Hui, Q. Ren, Three members of Ras GTPase superfamily are response to white spot syndrome virus challenge in *Marsupenaeus japonicus*, Fish Shellfish Immunol. 55 (2016) 623–631.
[47] Q. Ren, J. Zhou, Y.P. Jia, X.W. Wang, X.F. Zhao, J.X. Wang, Cloning and characterization of Rap GTPase from the Chinese white shrimp *Fenneropenaeus chinensis*, Dev. Comp. Immunol. 36 (2012) 247–252.
[48] M.T. Abreu-Blanco, J.M. Verboon, S.M. Parkhurst, Coordination of Rho family GTPase activities to orchestrate cytoskeleton responses during cell wound repair, Curr. Biol. 24 (2014) 144–155.
[49] K. Okkenhaug, B. Vanhaesebroeck, PI3K in lymphocyte development, differentiation and activation, Nat. Rev. Immunol. 3 (2003) 317–330.
[50] I. S, L. BL, Recent advances in the innate immunity of invertebrate animals, J. Biochem. Mol. Biol. 38 (2005) 128–150.
[51] Y. Sun, X. Zhang, G. Wang, S. Lin, X. Zeng, Y. Wang, et al., PI3K-AKT signaling pathway is involved in hypoxia/thermal-induced immunosuppression of small abalone *Haliotis diversicolor*, Fish Shellfish Immunol. 59 (2016) 492–508.
[52] X.-Y. Zhang, M.-Z. Zhang, C.-J. Zheng, J. Liu, H.-J. Hu, Identification of two hsp90 genes from the marine crab, *Portunus trituberculatus* and their specific expression profiles under different environmental conditions, Comp. Biochem. Physiol. C Toxicol. Pharmacol. 150 (2009) 465–473.
[53] H. Liu, J. Wu, M. Xu, J. He, A novel biomarker for marine environmental pollution of HSP90 from *Mytilus coruscus*, Mar. Pollut. Bull. 111 (2016) 428–434.
[54] J.-S. Rhee, I.T. Yu, B.-M. Kim, C.-B. Jeong, K.-W. Lee, M.-J. Kim, et al., Copper induces apoptotic cell death through reactive oxygen species-triggered oxidative stress in the intertidal copepod *Tigriopus japonicus*, Aquat. Toxicol. 132 (2013) 182–189.
[55] A. VB, T. RJ, Corneal epithelial wound healing, J. Biol. Syst. 03 (2003).
[56] A.D. Theocharis, S.S. Skandalis, C. Gialeli, N.K. Karamanos, Extracellular matrix structure, Adv. Drug Deliv. Rev. 97 (2016) 4–27.
[57] S. C, Extracellular matrix remodelling and cellular differentiation, Curr. Opin. Cell Biol. 11 (1999) 634.
[58] D.M. Levin, L.N. Breuer, S. Zhuang, S.A. Anderson, J.B. Nardi, M.R. Kanost, A hemocyte-specific integrin required for hemocytic encapsulation in the tobacco hornworm, Manduca sexta, Insect Biochem Molec 35 (2005) 369–380.
[59] I. Mamali, I. Lamprou, F. Karagiannis, M. Karakantza, M. Lampropoulou, V.J. Marmaras, A β integrin subunit regulates bacterial phagocytosis in medfly haemocytes, Dev. Comp. Immunol. 33 (2009) 858–866.
[60] K. Du, M. Montminy, CREB is a regulatory target for the protein kinase Akt/PKB, J. Biol. Chem. 273 (1998) 32377–32379.
[61] H. Grüneberg, A search for causes of polymorphism in *Clithon oualaniensis* (Lesson) (Gastropoda; Prosobranchia), Proc. Roy. Soc. Lond. 203 (1979) 379–386.
[62] X. Liu, S. Dong, C. Jin, Z. Bai, G. Wang, J. Li, Silkmapin of *Hyriopsis cumingii*, a novel silk-like shell matrix protein involved in nacre formation, Gene 555 (2015) 217–222.

[63] M. Suzuki, H. Nagasawa, An acidic matrix protein, Pif, is a key macromolecule for nacre formation, Science 325 (2009) 1388–1390.
[64] F. Badariotti, C. Lelong, M.P. Dubos, P. Favrel, Identification of three singular glycosyl hydrolase family 18 members from the oyster *Crassostrea gigas*: structural characterization, phylogenetic analysis and gene expression, Comp. Biochem. Physiol. B Biochem. Mol. Biol. 158 (2011) 56–63.
[65] G.L. Wang, B. Xu, Z.Y. Bai, J.L. Li, Two chitin metabolic enzyme genes from *Hyriopsis cumingii*: cloning, characterization, and potential functions, Genet. Mol. Res. 11 (2012) 4539.
[66] H.F. Zheng, Z.Y. Bai, J.Y. Lin, G.L. Wang, J.L. Li, Characterization and functional analysis of a chitin synthase gene (HcCS1) identified from the freshwater pearlmussel *Hyriopsis cumingii*, Genet. Mol. Res. 14 (2015) 19264.
[67] X. Liu, J. Li, L. Xiang, J. Sun, G. Zheng, G. Zhang, et al., The role of matrix proteins in the control of nacreous layer deposition during pearl formation, Proceedings Biological sciences 279 (2012) 1000–1007.
[68] L. Addadi, D. Joester, F. Nudelman, S. Weiner, Mollusk shell formation: a source of new concepts for understanding biomineralization processes, Chem. Eur J. 12 (2010) 980–987.
[69] J.Y. Lin, K.Y. Ma, Z.Y. Bai, J.L. Li, Molecular cloning and characterization of perlucin from the freshwater pearl mussel, *Hyriopsis cumingii*. Gene. 526 (2013) 210–216.